COMMUNICATION

Single-Crystalline V_2O_5 Ultralong Nanoribbon Waveguides

By *Bin Yan, Lei Liao, Yumeng You, Xiaojing Xu, Zhe Zheng, Zexiang Shen, Jan Ma, Limin Tong,* and *Ting Yu**

High-density photonic and optoelectronic integration is a natural alternative to electronic infrastructure and is a rapidly growing field.[1] Compared to traditional electrical transmission, optical transmission has a very large bandwidth (information capacity) and high speed. Central to progress in this area has been the development of materials and structures that can provide flexibility in connecting various nanophotonic elements. Conventionally, nanoscaled optical fibers are fabricated using a physical drawing process, and have been shown to be promising materials for low-loss optical guiding[2] and fast detection[3]. Admirable results presented by Yang and coworkers[4] demonstrate that single-crystalline semiconducting nanoribbons can be successfully used for passive and active photonic integrations. In addition, Lieber's group[5] reported that active nanowires have unique advantages in combination with electronics. Therefore, the fabrication of 1D single-crystal nanomaterials is of great scientific interest and technological significance, which will bring about the impetus of photonic integration and promote the development of optical information technology.

Divanadium pentoxide (V_2O_5), the most stable form in the vanadium oxide family, has been at the forefront of applied research due to its unique physical and chemical properties. For example, Gu and coworkers[6] showed that sheets made of entangled vanadium oxide nanofibres behave like artificial muscles (actuators) that contract reversibly under an electrical signal. In addition to its electromechanical properties, V_2O_5 also exhibits excellent photochromic or electrochromic behavior[7] upon light irradiation or electrochemical reactions. A number of enabling mechanical and optical properties show that the low-dimensional nanostructures of V_2O_5 are candidate materials for applications in photonics. In this regard, the optical properties of individual V_2O_5 nanoribbons are desirable and significant for our study.

There are several approaches available for synthesizing nanostructures of vanadium oxides.[8] It is important to develop a new method with desirable practical attributes, such as simplicity, catalyst-free, and not requiring extreme pressure conditions.[9] In this contribution, we have synthesized divanadium pentoxide nanoribbons using a simple thermal vapor deposition technique under ambient conditions. Representative dark-field optical images (Fig. 1a) revealed that nanoribbons with a typical length of several hundred micrometers, and even up to millimeters, were produced in high yield. The typical topography of the as-grown products was examined using field-emission scanning electron microscopy (SEM, JEOL JSM-6700F), as shown in Figure 2a. The ribbons have a rectangular cross-section with a typical width and height of ≈300 nm and ≈100 nm, respectively, giving a length-to-width or length-to-height aspect ratio of well over 1000. These nanostructures have excellent cross-section uniformity and smooth surfaces without pronounced structural defects, making them ideal for low-loss optical waveguides, sensors and interconnects.

Earlier works described the complicated structure of V_2O_5 as layer slabs of distorted trigonal bipyramids interconnected by shared edges and corners parallel to the (ab) layers.[10] The room-temperature Raman spectrum (Fig. 2b) of a V_2O_5 sample exhibits bands at 143, 198, 286, 306, 406, 483, 526, 702, and 996 cm^{-1}, which are characteristic modes for this compound.[11] High-frequency Raman peaks at 996 cm^{-1} and 702 cm^{-1}

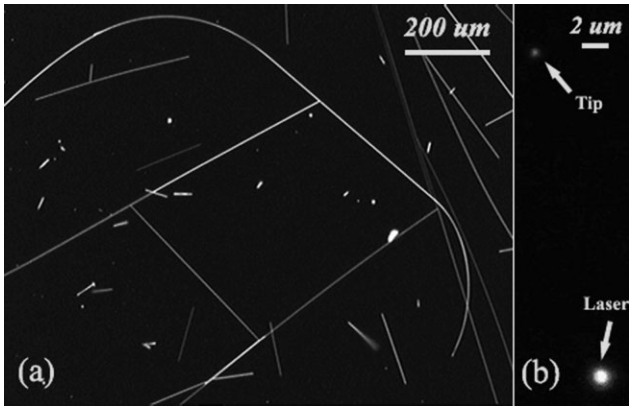

Figure 1. Optical waveguiding effects in V_2O_5 nanoribbons. a) Dark-field image of an as-grown sample. b) Far-field photoluminescence image of a nanoribbon waveguide under laser excitation. The laser is focused to a spot size of 500 nm at the middle of the ribbon. Generated PL (in bottom right corner) is guided to the tip of the ribbon (in top left corner).

[*] Prof. T. Yu, B. Yan, L. Liao, Y. M. You, Z. Zheng, Prof. Z. X. Shen
Division of Physics and Applied Physics
School of Physical and Mathematical Sciences
Nanyang Technological University
Singapore 637371 (Singapore)
E-mail: yuting@ntu.edu.sg
Dr. X. J. Xu, Prof. J. Ma
Division of Materials Technology
School of Materials Science and Engineering
Nanyang Technological University
Singapore 639798 (Singapore)
Prof. L. M. Tong
State Key Laboratory of Modern Optical Instrumentation
Zhejiang University
Hangzhou 310027 (China)

DOI: 10.1002/adma.200803684

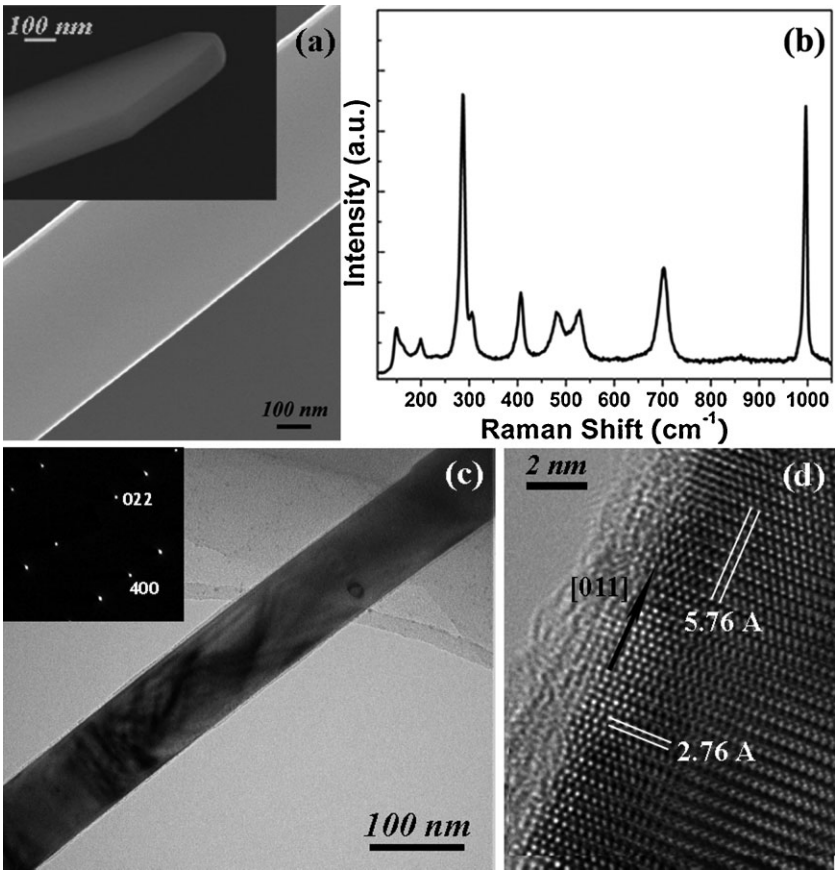

Figure 2. a) High-magnication SEM images of the sample. The inset shows the near-rectangular cross section of a V_2O_5 nanoribbon. b) Raman spectrum of an individual nanoribbon. c) Field-emission transmission electron microscopy (FETEM) image of an individual V_2O_5 nanoribbon with its corresponding SAED pattern. d) High-magnification TEM image.

correspond to the stretching modes of the V=O (terminal oxygen) and V_2–O (doubly coordinated oxygen) bonds respectively. The peak at 526 cm^{-1} is assigned to the V_3–O (triply coordinated oxygen) stretching mode. The peaks locating at 406 and 286 cm^{-1} are assigned to the bending vibration of the V=O bonds; while those at 483 and 306 cm^{-1} are assigned to the bending vibrations of V–O–V (bridging doubly coordinated oxygen) and V_3–O (triply coordinated oxygen) bonds, respectively. Transmission electron microscope (TEM) images (Fig. 2c) reveal the morphology of the nanostructure. The top inset shows the corresponding selected-area electron diffraction (SAED) pattern confirming the growth of single-crystalline V_2O_5 in the [011] direction. Here, the brightest central spot in SAED is blocked in order to get a better contrast. The lattice-resolved image (Fig. 2d) of a typical nanoribbon reveals the single-crystalline nature of the sample.

A 457 nm laser was used to study the waveguiding properties of the as-grown V_2O_5 nanoribbons. Figure 1b shows an optical microscopy image of the samples with a notch-filter. Only part of the nanoribbon is shown in this figure because of the limited imaging area of the CCD. Significantly, the emission of the sample under laser excitation was so strong that it could be imaged easily with a color CCD camera (768 pixel × 576 pixel). The large bright facula in the bottom right-hand corner of the image is the in situ photoluminescence (PL) under laser illumination. Notable bright luminescence spots were observed at the end of the nanoribbon irrespective of the position of excitation on the sample, which is due to the waveguided PL emission scattering at the tip. The localization of the out-coupling of the light at the ends of each wire is a typical feature of the strong optical waveguiding behavior. In contrast, the body of sample is not visible in the optical image, showing that the V_2O_5 nanoribbons are promising low-loss components for photonic devices in the micrometer or nanometer scale. The effective waveguide behavior is attributed to the large difference between the refractive index of the nanostructure ($n_{V_2O_5} = 2.3$) and those of the external media ($n_{air} = 1$ and $n_{SiO_2} = 1.45$), which results in tight optical confinement in the ribbons.

The dependence of the intensity of out-coupled luminescence at the rightmost tip of an unoptimized nanoribbon (width: ≈320 nm, length: ≈100 μm) on propagation length is shown in Figure 3a. Considering the small fluctuations in excitation power, the measured intensities at the end-faces are normalized against those measured at each excitation location on the nanoribbon body. These data (Fig. 3b) can be well-fitted by a first-order exponential decay function, expressed by $I_{tip}/I_0 = \exp(-\alpha x)$, where I_{tip} is the luminescent intensity measured at the tip, I_0 is the normalized intensity at the excitation spot, x is the propagation length and α is a fitting parameter. The propagation loss is about 0.06 dB μm^{-1}, which is much lower than the optical loss of other sub-wavelength structures such as metallic plasmon waveguides (≈1 dB μm^{-1})[12] and organic nanowires (0.3 dB μm^{-1})[13]. And the effective waveguiding properties can be attributed to the good crystalline quality. However, the optical

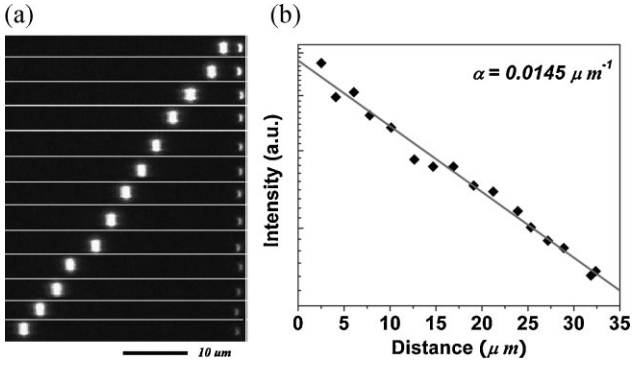

Figure 3. a) PL images of a single nanoribbon. PL images were collected upon excitation of the identical ber at different positions. b) Normalized dependence of the tip out-coupled emission intensity on excitation location. The line is an exponential fit to the data yielding the loss coefficient for the waveguide.

loss is still larger than the reports in refs. [2] and [4]. Some sources for the propagation losses will be discussed later.

To obtain further insight to the light propagation behavior of the sample, the V_2O_5 nanoribbons were transferred onto a cover glass substrate (thickness: 0.17 mm), and the PL spectra of the emitted light with respect to the distance between the excitation point and the end of nanoribbon were investigated using a WITEC CRM200 Raman system. The setup is shown in Figure 4a (see Experimental Section). Figure 4b displays the spectra of the waveguided emission that is out-coupled at the tip as a function of increasing propagation length. The nanoribbon exhibits room-temperature luminescence in the 550–750 nm region, with a full-width at half-maximum (FWHM) of approximately 96 nm. This broad PL spectrum may help in manipulating light in the waveguides.[5,8f] As shown in Figure 4b, the intensity of the long-wavelength side of the PL decreases significantly with an increase in the guided distance, which results in a continuous blue-shift of the spectra. The absorption measurements (in Fig. 4b) allow us to infer two important points about the sample. First, considering the band-gap (≈2.3 eV) of V_2O_5, the above-mentioned visible-light emissions, obviously, should not be reabsorbed by interband transitions along the fiber. Light with longer wavelengths tends to suffer higher evanescent leakage due to the decrease in optical confinement with increasing free-space wavelength.[14] Second, a small absorption tail can be observed at about 700 nm. This low-energy absorption is associated with transitions involving impurity states within the energy gap, that is, V^{4+} ions.[15] Such kind of native-defects levels are probably related to the absorption in the long-wavelength range. Overall, our data indicate that nanoribbons can be made into reasonably good short-pass filters with tunable cutoffs based on path length, by exploiting evanescent leakage and impurity-state absorption.[4a] Besides, we note that other experiment parameters, such as light polarization, wavelength, and fiber diameter, also affect

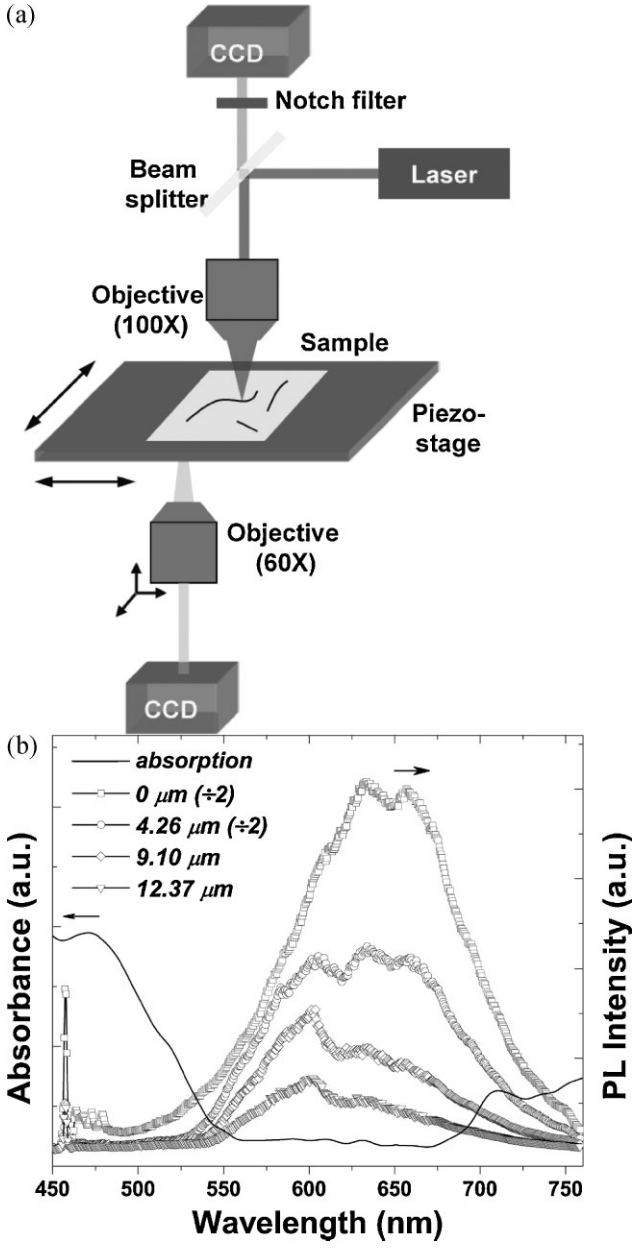

Figure 4. Measurement of the waveguide characteristics of the nanoribbons. a) Schematic illustration of the experimental setup. b) Absorption and waveguided PL spectra of a V_2O_5 nanoribbon. The waveguided PL was captured at various excitation/tip distances.

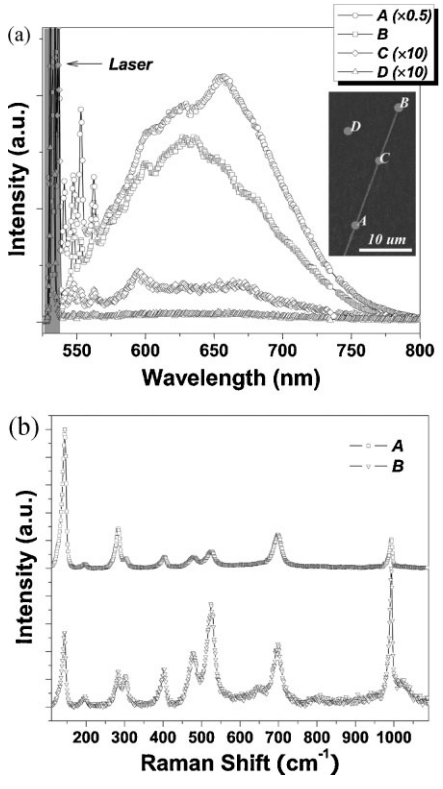

Figure 5. a) Spatially resolved emission spectra recorded at different positions of a sample. The inset shows the locations of the collecting points, *A*: excitation point; *B*: tip of nanoribbon; *C*: body of the ribbon; *D*: background. b) Corresponding Raman signals from collection points *A* and *B*.

the performance of these nanoribbons for such functions, which need further study.

In addition to the above-mentioned nanoscale active optical waveguides, we were also interested in exciting Raman-active modes in the waveguides by launching 532 nm light down the V_2O_5 cavities (near resonance Raman scattering[16]). The light undergoes Raman scattering from molecules in the material, and this is expected to give rise to the Stokes shifted lines at longer wavelengths. Figure 5 shows that the peak positions detected at the tip (B) correspond well to the Raman spectra collected at the excitation point (A), accompanying the PL band of V_2O_5. No significant broadening was observed in the Raman signal. The fluorescence spectrum from the body (C) was also observed, and was ascribed to some inevitable surface contaminants. These contaminants may scatter the guided light, which results in a lower waveguiding efficiency. More importantly, we found that certain Raman signals collected at the tip, especially the peaks at around 550 and 1000 cm^{-1}, become dominant due to the transfer of energy from near-resonant excitation to those at longer wavelengths, and thus amplifies the Raman signals. In fact, the Raman Stokes power is comparable to the broadband emission of the sample. This Raman-active effect described for V_2O_5 nanoribbons is extremely important in optical-fiber communication systems and as devices on their own. The basic function demonstrated in this work may open up opportunities in Raman nanofiber amplifiers/lasers and other compact analytical devices. Indeed, stimulated Raman scattering in Si waveguides and Raman amplifier integrated with an external fiber-based optical feedback have been demonstrated to yield optically pumped Raman lasing in Si.[17]

In summary, we have reported the synthesis of single-crystalline divanadium pentoxide nanoribbons using a simple thermal vapor deposition technique. Considering the smooth surface and high refractive index that give rise to the tight optical confinement, it is the first demonstration of efficient light propagation in V_2O_5 nanoribbons. The results provide useful information for the construction of future nanoscaled waveguide structures. Regular V_2O_5 waveguides were found to exhibit Raman signals with near-resonance excitation and guide these modes through the nanoribbon cavity. The initial results shown here provide experimental support for the development of novel nanophotonic elements. Further work is in progress to fully explore the optical behaviors of these nanoribbons, especially with respect to their potential to exhibit nonlinear properties and sensing.

Experimental

A clean piece of vanadium foil (10 mm × 10 mm × 0.1 mm) with a purity of 99.8% (Lesker) was heated at 660 °C under ambient conditions with a piece of Si wafer (with a 200 nm thick, thermally grown SiO_2 layer) covering the foil without the use of catalyst. After the heating process of about 6 h, the sample was allowed to cool down to room temperature before removal from the furnace. Elongated nanostructures were observed on the side of the wafer facing the metal foil.

The optical waveguiding properties were investigated using a WITEC CRM200 Raman system. The setup is shown in Figure 4a. The excitation laser ($\lambda = 457$ nm or 532 nm) was focused onto the sample using a 100× optical lens (NA = 0.95). The laser spot size was around 500 nm in diameter. The piezostage movement and data acquisition were controlled using ScanCtrl Spectroscopy Plus software from WITec GmbH, Germany. The detected light was captured from the opposite side of the substrate with a 60× cover-glass-corrected objective lens (NA = 0.80), which can be motorized in three dimensions. The signals collected were routed to a TE-cooled charge-coupled-device (CCD) cooled to −64 °C. With this technique, the procession of light traveling along the fiber can be effectively studied by moving the stage and collection lens. The absorption spectrum of the sample was acquired using a Varian Cary 100 UV-Vis spectrophotometer. All measurements were performed at room temperature.

Acknowledgements

The author would like to thank C. P. Wong for her beneficial discussion. L. L. acknowledges support in this work by the Singapore Millennium Foundation 2008 scholarship.

Received: December 13, 2008
Revised: January 16, 2009
Published online: March 23, 2009

[1] a) Y. Nakayama, P. J. Pauzauskie, A. Radenovic, R. M. Onorato, R. J. Saykally, J. Liphardt, P. Yang, *Nature* **2007**, *447*, 1098. b) X. F. Duan, Y. Huang, R. Agarwal, C. M. Lieber, *Nature* **2003**, *421*, 241. c) D. J. Sirbuly, M. Law, H. Yan, P. Yang, *J. Phys. Chem. B* **2005**, *109*, 15190. d) R. Agarwal, C. M. Lieber, *Appl. Phys. A* **2006**, *85*, 209.

[2] a) L. Tong, R. R. Gattass, J. B. Ashcom, S. He, J. Lou, M. Shen, I. Maxwell, E. Mazur, *Nature* **2003**, *426*, 816. b) L. Tong, J. Lou, R. R. Gattass, S. He, X. Chen, L. Liu, E. Mazur, *Nano Lett.* **2005**, *5*, 259. c) X. Xing, H. Zhu, Y. Wang, B. Li, *Nano Lett.* **2008**, *8*, 2839.

[3] F. Gu, L. Zhang, X. Yin, L. Tong, *Nano Lett.* **2008**, *8*, 2757.

[4] a) M. Law, D. J. Sirbuly, J. C. Johnson, J. Goldberger, R. J. Saykally, P. Yang, *Science* **2004**, *305*, 1269. b) D. J. Sirbuly, M. Law, P. Pauzauskie, H. Yan, A. V. Maslov, K. Knutsen, C.-Z. Ning, R. J. Saykally, P. Yang, *Proc. Natl. Acad. Sci. USA* **2005**, *102*, 7800.

[5] a) C. J. Barrelet, A. B. Greytak, C. M. Lieber, *Nano Lett.* **2004**, *4*, 1981. b) A. B. Greytak, C. J. Barrelet, Y. Li, C. M. Lieber, *Appl. Phys. Lett.* **2005**, *87*, 151103.

[6] G. Gu, M. Schmid, P.-W. Chiu, A. Minett, J. Fraysse, G.-T. Kim, S. Roth, M. Kozlov, E. Munoz, R. H. Baughman, *Nat. Mater.* **2003**, *2*, 316.

[7] a) S. Nishio, M. Kakihana, *Chem. Mater.* **2002**, *14*, 3730. b) C. Xiong, A. E. Aliev, B. Gnade, K. J. Balkus, *ACS Nano* **2008**, *2*, 293.

[8] a) N. Pinna, M. Willinger, K. Weiss, J. Urban, R. Schlögl, *Nano Lett.* **2003**, *3*, 1131. b) H.-J. Muhr, F. Krumeich, U. P. Schönholzer, F. Bieri, M. Niederberger, L. J. Gauckler, R. Nesper, *Adv. Mater.* **2000**, *12*, 231. c) G. R. Patzke, F. Krumeich, R. Nesper, *Angew. Chem. Int. Ed.* **2002**, *41*, 2446. d) F. Krumeich, H.-J. Muhr, M. Niederberger, F. Bieri, B. Schnyder, R. Nesper, *J. Am. Chem. Soc.* **1999**, *121*, 8324. e) P. M. Ajayan, O. Stephan, P. Redlih, C. Colliex, *Nature* **1995**, *375*, 564. f) N. Hullavarad, S. Hullavarad, P. C. Karulkar, *J. Electrochem. Soc.* **2008**, *155*, K84.

[9] a) T. Yu, Y. Zhu, X. Xu, K. Yeong, Z. Shen, P. Chen, C. Lim, J. Thong, C. Sow, *Small* **2006**, *2*, 80. b) M. Reddy, T. Yu, C. Sow, Z. Shen, C. Lim, G. V. Subba Rao, B. Chowdari, *Adv. Funct. Mater.* **2007**, *17*, 2792. c) Z. Zheng, B. Yan, Y. You, J. Zhang, Z. X. Shen, C.-T. Lim, T. Yu, *Adv. Mater.* **2008**, *20*, 352.

[10] a) R. Enjalbert, J. Galy, *Acta Crystallogr. Sect. C* **1986**, *42*, 1467. b) V. Eyert, K.-H. Hock, *Phys. Rev. B* **1998**, *57*, 12727.

[11] a) A. G. Souza Filho, O. P. Ferreira, E. J. G. Santos, J. Mendes Filho, O. L. Alves, *Nano Lett.* **2004**, *4*, 2099. b) L. Abello, E. Husson, Y. Repelin, G. Lucazeau, *Spectrochim. Acta Part A* **1983**, *39*, 641.

[12] a) S. A. Maier, P. G. Kik, H. A. Atwater, *Appl. Phys. Lett.* **2002**, *81*, 1714. b) M. Yan, L. Thylen, M. Qiu, D. Parekh, *Opt. Express* **2008**, *16*, 7499.

[13] D. O'Carroll, I. Lieberwirth, G. Redmond, *Small* **2007**, *3*, 1178.

[14] A. W. Snyder, J. D. Love, *Optical Waveguide Theory*, Chapman and Hall, Landon **1983**.
[15] M. Benmoussa, E. Ibnouelghazi, A. Bennouna, E. L. Ameziane, *Thin Solid Films* **1995**, *265*, 22.
[16] a) J.-C. Panitz, A. Wokaun, *J. Phys. Chem.* **1996**, *100*, 18357. b) A. K. Arora, A. K. Ramdas, *Phys. Rev. B* **1987**, *35*, 4345. c) M. Dieterle, G. Weinberg, G. Mestl, *Phys. Chem. Chem. Phys.* **2002**, *4*, 812. d) P. Y. Yu, C. Hermann, *Phys. Rev. B* **1981**, *23*, 4097. e) L. G. Cancado, M. A. Pimenta, R. Saito, A. Jorio, L. O. Ladeira, A. Grueneis, A. G. Souza-Filho, G. Dresselhaus, M. S. Dresselhaus, *Phys. Rev. B* **2002**, *66*, 035415.
[17] a) R. Claps, D. Dimitropoulos, Y. Han, B. Jalali, *Opt. Express* **2002**, *10*, 1305. b) R. Claps, D. Dimitropoulos, V. Raghunathan, Y. Han, B. Jalali, *Opt. Express* **2003**, *11*, 1731. c) H. Rong, A. Liu, R. Jones, O. Cohen, D. Hak, R. Nicolaescu, A. Fang, M. Paniccia, *Nature* **2005**, *433*, 292. d) H. Rong, S. Xu, Y.-H. Kuo, V. Sih, O. Cohen, O. Raday, M. Paniccia, *Nat. Photon.* **2007**, *1*, 232.